

A renormalization group method for studying the early universe in the Lorentzian IIB matrix model

Yuta Ito^{1,*}, Sang-Woo Kim^{2,*}, Yuki Koizuka^{1,*}, Jun Nishimura^{1,3,*} and Asato Tsuchiya^{4,*}

¹*Department of Particle and Nuclear Physics,
Graduate University for Advanced Studies (SOKENDAI),
Tsukuba, Ibaraki 305-0801, Japan*

²*School of Physics, Korea Institute for Advanced Study (KIAS),
85 Hoegiro Dongdaemun-gu, Seoul 130-722, Korea*

³*Theory Center, High Energy Accelerator Research Organization (KEK),
Tsukuba, Ibaraki 305-0801, Japan*

⁴*Department of Physics, Shizuoka University,
836 Ohya, Suruga-ku, Shizuoka 422-8529, Japan*

**E-mail: yito@post.kek.jp, sang@kias.re.kr, koizuka@post.kek.jp,
jnishi@post.kek.jp, satsuch@ipc.shizuoka.ac.jp*

.....
We propose a new method for studying the early universe in the Lorentzian version of the IIB matrix model, which is considered to be a nonperturbative formulation of superstring theory. This method is based on the idea of renormalization group, and it enables us to study the time-evolution of the universe for much longer time than in the previous work, which showed that the SO(9) rotational symmetry is spontaneously broken down to SO(3) after a “critical time”. We demonstrate how this method works in a simplified model, which is expected to capture the behaviors of the original model when the space is not so large. In particular, we present clear evidence that the three-dimensional space expands *exponentially* after the critical time in this simplified model.
.....

Subject Index B25

1. Introduction

Understanding how our universe began is one of the most fundamental and fascinating themes in theoretical physics. For instance, there are good reasons to believe that our universe underwent a rapid expansion called inflation before the Big Bang. While there are various models which describe inflation phenomenologically, we still do not have a description based on first-principle calculations in a complete quantum gravity theory like superstring theory. The most crucial problem with superstring theory is that it is defined only perturbatively around consistent backgrounds, and within such perturbative formulations, it is known that the cosmic singularity is not resolved generally [1–4]. In order to overcome this problem, one really needs to use a fully nonperturbative formulation. In fact, there exist concrete proposals for such a formulation using supersymmetric matrix models [5–7]. These models

can be obtained *formally*¹ by dimensionally reducing ten-dimensional $\mathcal{N} = 1$ super Yang-Mills theory to $d = 0, 1, 2$ dimensions, respectively. Based on these proposals, various issues of the early universe have been discussed [8–17]. As a closely related direction, ref. [18] proposes a conformal field theory, which is holographically dual to inflationary models. (See also ref. [19] and references therein.)

The IIB matrix model [5] is one of the matrix model proposals corresponding to the $d = 0$ case mentioned above,² in which not only space but also time should emerge dynamically from the matrix degrees of freedom. This aspect of the IIB matrix model has also been discussed intensively as “emergent gravity” [21–28] in noncommutative field theories, which appear in the IIB matrix model for a particular class of classical backgrounds [29–32]. (See also ref. [33] for a different proposal for emergence of curved space-time in the matrix model.) Until quite recently, the IIB matrix model was studied after making a Wick rotation since the partition function of the Euclidean matrix model obtained in this way was shown to be finite [34, 35]. In fact, a lot of efforts have been devoted to identifying the matrix configurations that dominate the partition function using various methods [36–50]. However, the Euclidean matrix model is clearly not applicable to cosmology since it does not provide the real-time dynamics. Moreover, it is known that the Wick rotation is more subtle in quantum gravity than in quantum field theory at the nonperturbative level (See, for instance, refs. [51, 52]). Indeed a recent study based on the Gaussian expansion method suggests that the space-time obtained dynamically in the Euclidean matrix model does not seem to correspond to our four-dimensional space-time [50].

Motivated by all these problems with the Euclidean IIB matrix model, three of the authors (S.-W.K., J.N. and A.T.) studied the Lorentzian version of the IIB matrix model by Monte Carlo simulation for the first time [53]. Unlike the Euclidean version, one has to introduce infrared cutoffs in both spatial and temporal directions in order to make the partition function finite. However, it was found that these two cutoffs can be removed in the large- N limit in such a way that physical quantities scale. The eigenvalue distribution of the matrix representing the time extends in that limit, and the dominant matrix configurations have a very nontrivial structure, which enables us to naturally extract the time-evolution. Quite surprisingly, it was found that a phase transition occurs at some point in time, and after that, only three out of nine spatial directions start to expand. This phase transition can be interpreted as the birth of our 3-dimensional universe in superstring theory. It should be emphasized that the results seem to suggest that the space-time dimensionality is determined *uniquely* by the nonperturbative dynamics of superstrings unlike in perturbative string theory, in which consistent backgrounds can have various space-time dimensionality.

As another important property of the Lorentzian IIB matrix model, it is expected that the classical approximation becomes valid at late times [54, 55]. The reason for this is that each term in the action has large contribution from the degrees of freedom at late times due to the expansion of the universe. One can actually construct a simple solution representing an expanding (3+1)-dimensional universe, which naturally solves the cosmological constant

¹ Note that ten-dimensional $\mathcal{N} = 1$ super Yang-Mills theory is not well-defined at the quantum level due to gauge anomaly. The relationship between the matrix models and the 10-dimensional super Yang-Mills theory actually refers only to that of the classical action.

² See ref. [20] for a review of recent developments in the IIB matrix model.

problem [55]. It has also been argued that local field theory emerges from low-lying fluctuation modes around a solution representing a commutative space-time [56]. In fact, the classical equations of motion of the matrix model have infinitely many solutions, which is reminiscent of the so-called landscape in superstring theory. Unlike the situation with the landscape, however, there is a definite criterion to pick up a particular solution describing the late-time behaviors since we have a well-defined partition function.

Clearly it is important to extend the Monte Carlo studies in ref. [53] to much longer time. For instance, it would be interesting to see whether the inflation and the Big Bang occurs in this model as is generally believed in modern cosmology. Moreover, if we can go further and reach the time region in which the classical approximation is valid, we should be able to determine the solution which actually describes the late-time behaviors in the dominant configurations. Once this has been done, we should be able to derive the effective field theory below the scale where gravity decouples by considering the fluctuations around the classical solution. In particular, it would be interesting to see whether the Standard Model particles appear at low energy, for instance, in a way speculated in refs. [57–60].

To this end, we develop a new method that enables us to investigate a long time-evolution of the universe in the Lorentzian IIB matrix model by Monte Carlo simulation. Note, in particular, that the time scale that one would hope to achieve is, at least, a few orders of magnitude larger than the typical time scale of the model. If one attempts to study it directly, one would need a huge matrix size, which makes the calculation impractical. In this paper we show that there exists a “renormalized theory”, which corresponds to a theory obtained from the original model by integrating out the dynamical degrees of freedom at earlier times. The renormalized theory has two extra parameters compared with the original model, which can be used to optimize the length of the time region that one can actually probe. By simulating the renormalized theory with optimized parameters, we can investigate the late-time behaviors with much less dynamical degrees of freedom than the direct approach would require.

In order to show how the method works, we consider a simplified model, which can be obtained from the original model by neglecting the coupling of fermionic matrices to the spatial bosonic matrices. This approximation is expected to be valid at early times, where the space is not so large. Then the Pfaffian that arises from integrating out fermionic matrices can be expressed by some power of the van der Monde determinant, which is written explicitly in terms of the eigenvalues of the temporal matrix only, and the simulation becomes as fast as the bosonic model. The simplified model indeed retains the important properties of the original model such as the spontaneous breaking of the rotational symmetry at some critical time. Moreover, we find that the size of the universe grows exponentially after the critical time. We apply the renormalization group method to the simplified model and confirm the exponential expansion more clearly with smaller matrices.

The rest of the paper is organized as follows. In section 2 we review some important properties of the Lorentzian IIB matrix model. In section 3 we define the simplified model, and present results obtained by direct Monte Carlo studies. In particular, we show that the exponential expansion is realized in this model after the spontaneous breaking of rotational symmetry. In section 4 we describe the renormalization group method. In section 5 we apply the method to the simplified model and show that it allows us to study the time-evolution

much more efficiently. Section 6 is devoted to a summary and discussions. In appendix A we derive the form of the model suitable for Monte Carlo simulation. In appendix B we give some details of our Monte Carlo simulation.

2. Brief review of the Lorentzian IIB matrix model

The IIB matrix model has an action [5]

$$S = S_b + S_f , \quad (2.1)$$

$$S_b = -\frac{1}{4g^2} \text{Tr} \left([A_\mu, A_\nu] [A^\mu, A^\nu] \right) , \quad (2.2)$$

$$S_f = -\frac{1}{2g^2} \text{Tr} \left(\Psi_\alpha (C\Gamma^\mu)_{\alpha\beta} [A_\mu, \Psi_\beta] \right) , \quad (2.3)$$

where the bosonic $N \times N$ matrices A_μ ($\mu = 0, \dots, 9$) and the fermionic ones Ψ_α ($\alpha = 1, \dots, 16$) are both traceless and Hermitian. Γ^μ are 10-dimensional gamma-matrices after the Weyl projection and \mathcal{C} is the charge conjugation matrix. Since the coupling constant g can be absorbed by rescaling A_μ and Ψ appropriately, it is merely a scale parameter.

The IIB matrix model is conjectured to be a nonperturbative definition of superstring theory [5]. There are various pieces of evidence for this conjecture. First of all, the action (2.1) can be regarded as a matrix regularization of the worldsheet action of type IIB superstring theory in the Schild gauge [5].³ Secondly, D-branes in type IIB superstring theory can be described in the matrix model, and the interaction between them can be correctly reproduced [5]. Thirdly, under a few reasonable assumptions, the string field Hamiltonian for type IIB superstring theory can be derived from Schwinger-Dyson equations for the Wilson loop operators, which are identified as creation and annihilation operators of strings [61].

In all these connections to type IIB superstring theory, the target space coordinates are identified with the eigenvalues of the matrices A_μ . In particular, this identification is consistent with the supersymmetry algebra of the model, in which the translation that appears from the anti-commutator of supersymmetry generators is identified with the shift symmetry $A_\mu \mapsto A_\mu + \alpha_\mu \mathbf{1}$ of the model,⁴ where $\alpha_\mu \in \mathbf{R}$. Also the fact that the model has extended $\mathcal{N} = 2$ supersymmetry in ten dimensions is consistent with the fact that the model actually includes gravity since it is known in field theory that $\mathcal{N} = 1$ supersymmetry is the maximal one that can be achieved in ten dimensions without including gravity.

The partition function for the Lorentzian version of the IIB matrix model is proposed as [53]

$$Z = \int dA d\Psi e^{iS} . \quad (2.4)$$

Integrating out the fermionic matrices, we obtain the Pfaffian

$$\text{Pf} \mathcal{M}(A) = \int d\Psi e^{iS_f} , \quad (2.5)$$

³ This does not imply that the matrix model is merely a formulation for the “first quantization” of superstrings. In fact, multiple worldsheets appear naturally in the matrix model as block-diagonal configurations, where each block represents the embedding of a single worldsheet into the 10-dimensional target space.

⁴ Apparently, this symmetry is not consistent with the traceless condition on A_μ . For a more precise argument, one should consider a block diagonal configuration and shift each block relatively [5].

which is real. Note that the bosonic action (2.2) can be written as

$$S_b = \frac{1}{4g^2} \text{Tr}(F_{\mu\nu} F^{\mu\nu}) \quad (2.6)$$

$$= \frac{1}{4g^2} \{ -2 \text{Tr}(F_{0i})^2 + \text{Tr}(F_{ij})^2 \} , \quad (2.7)$$

where we have defined Hermitian matrices $F_{\mu\nu} = i[A_\mu, A_\nu]$. Hence the bosonic action is not positive semi-definite.

The partition function (2.4) is not finite as it stands, but it can be made finite by introducing infrared cutoffs in both temporal and spatial directions as [53]

$$\frac{1}{N} \text{Tr}(A_0)^2 \leq \kappa \frac{1}{N} \text{Tr}(A_i)^2 , \quad (2.8)$$

$$\frac{1}{N} \text{Tr}(A_i)^2 \leq \Lambda^2 . \quad (2.9)$$

It turned out that these two cutoffs can be removed in the large- N limit in such a way that physical quantities scale. The resulting theory thus obtained has no parameter except one scale parameter.

After some manipulation and rescaling of A_μ (See Appendix A), the partition function can be rewritten as [53]

$$Z = \int dA \text{Pf} \mathcal{M}(A) \delta \left(\frac{1}{N} \text{Tr}(F_{\mu\nu} F^{\mu\nu}) \right) \delta \left(\frac{1}{N} \text{Tr}(A_i)^2 - L^2 \right) \theta \left(\kappa L^2 - \frac{1}{N} \text{Tr}(A_0)^2 \right) , \quad (2.10)$$

where $\theta(x)$ is the Heaviside step function and L is a scale parameter introduced for later convenience. Since the Pfaffian $\text{Pf} \mathcal{M}(A)$ is real unlike in the Euclidean case [40–42, 49], the model (2.10) can be studied by Monte Carlo simulation without the sign problem.⁵

Let us then discuss how we can extract the time-evolution from a configuration generated by simulating the system (2.10). First we choose the $SU(N)$ basis in such a way that the temporal matrix A_0 is diagonalized as

$$A_0 = \text{diag}(\alpha_1, \dots, \alpha_N) , \quad \text{where } \alpha_1 < \dots < \alpha_N . \quad (2.11)$$

In that basis, it turned out that the spatial matrices A_i has a band-diagonal structure with off-diagonal elements $(A_i)_{ab}$ for $|a - b| \geq n$ being small for some integer n . Therefore, we may naturally consider $n \times n$ block matrices

$$(\bar{A}_i)_{IJ}(t) \equiv (A_i)_{\nu+I, \nu+J} , \quad (2.12)$$

where $I, J = 1, \dots, n$ and $\nu = 0, 1, \dots, N - n$, as representing a state of the universe at the time

$$t = \frac{1}{n} \sum_{I=1}^n \alpha_{\nu+I} . \quad (2.13)$$

⁵ Strictly speaking, the Pfaffian is not positive semi-definite. However, it turns out that the configurations with positive Pfaffian dominate the partition function at large N . Therefore, we may simply replace the Pfaffian by its absolute value $|\text{Pf} \mathcal{M}(A)|$ in actual simulation [53].

For instance, the extent of space at time t is defined by

$$R^2(t) = \left\langle \frac{1}{n} \text{tr} (\bar{A}_i(t))^2 \right\rangle , \quad (2.14)$$

where the trace here is taken over the $n \times n$ block. In order to see the spontaneous breaking of SO(9) symmetry, we define the ‘‘moment of inertia tensor’’

$$T_{ij}(t) = \frac{1}{n} \text{tr} (\bar{A}_i(t) \bar{A}_j(t)) , \quad (2.15)$$

which is represented by a real symmetric 9×9 matrix. We denote the real positive semi-definite eigenvalues of $T_{ij}(t)$ as $\lambda_j(t)$ with the ordering

$$\lambda_1(t) > \lambda_2(t) > \cdots > \lambda_9(t) . \quad (2.16)$$

If the SO(9) symmetry is not spontaneously broken, the expectation values $\langle \lambda_i(t) \rangle$ become equal in the large- N (and large- n) limit. We find that this is indeed the case at early times, while at sufficiently late times, three of the eigenvalues become considerably larger than the others, suggesting that the SO(9) symmetry is spontaneously broken down to SO(3) after a critical time.

The necessity for introducing the cutoff (2.8) in the temporal direction can be understood as follows. Let us consider a situation in which the eigenvalues of A_0 are well separated from each other and estimate the effective action for the eigenvalues perturbatively. By fixing the gauge to (2.11), we rewrite the integration over A_μ as

$$\int dA = \int dA_i \int \prod_{a=1}^N d\alpha_a \Delta(\alpha)^2 , \quad (2.17)$$

$$\Delta(\alpha) \equiv \prod_{a>b}^N (\alpha_a - \alpha_b) , \quad (2.18)$$

where $\Delta(\alpha)$ is the van der Monde (VDM) determinant. The action can be expanded as

$$S_b = -\frac{1}{4g^2} (\alpha_a - \alpha_b)^2 |(A_i)_{ab}|^2 + \cdots , \quad (2.19)$$

$$S_f = -\frac{1}{2g^2} (\Psi_\alpha)_{ba} (\alpha_a - \alpha_b) (\mathcal{C}\Gamma^\mu)_{\alpha\beta} (\Psi_\beta)_{ab} + \cdots , \quad (2.20)$$

where the omitted terms are subleading for large $|\alpha_a - \alpha_b|$. Integrating out A_i at the one-loop level, one obtains $\Delta(\alpha)^{-18}$ neglecting the zero modes corresponding to diagonal elements. Integrating out Ψ_α at the one-loop level, one obtains $\Delta(\alpha)^{16}$ neglecting the zero modes. Thus one finds that the $\Delta(\alpha)^2$ in (2.17) is canceled exactly at the one-loop level, which is actually a consequence of the supersymmetry [5] of the model (2.4). Due to this property, the eigenvalue distribution of A_0 extends to infinity even for finite N if it were not for the cutoff (2.8).

3. A simplified model and its properties

The argument given above motivates us to generalize the Lorentzian IIB matrix model to $(d+1)$ -dimensional versions ($d=9, 5, 3$), which can be obtained by dimensional reduction of $(d+1)$ -dimensional $\mathcal{N}=1$ super Yang-Mills theory. (The $d=9$ case corresponds to the

Lorentzian IIB matrix model.) In general, integration over A_i gives $\Delta(\alpha)^{-2d}$, while integration over the fermionic matrices gives $\Delta(\alpha)^{2(d-1)}$. Hence the VDM determinant that appears as in (2.17) is canceled exactly at the one-loop level and there is no interaction among the eigenvalues of A_0 at the one-loop level. In Monte Carlo simulations, the eigenvalue distribution indeed extends to infinity if one does not introduce the temporal cutoff κ as in (2.8). If one omits fermions, one obtains an attractive force between the eigenvalues of A_0 , and the eigenvalue distribution of A_0 has a finite extent without any cutoff.

In fact, the $d = 5$ supersymmetric model turns out to have very similar properties as the original model.⁶ In particular, the $\text{SO}(5)$ rotational symmetry is broken spontaneously down to $\text{SO}(3)$ after a critical time. The $(5+1)$ -dimensional model contains bosonic matrices A_μ ($\mu = 0, \dots, 5$) and fermionic matrices Ψ_α and $\bar{\Psi}_\alpha$ ($\alpha = 1, \dots, 4$). The action for the fermionic matrices is given by

$$S_{\text{f},6\text{d}} = -\frac{1}{2g^2} \text{Tr} \left(\bar{\Psi}_\alpha (\Gamma^\mu)_{\alpha\beta} [A_\mu, \Psi_\beta] \right), \quad (3.1)$$

where Γ^μ are 6-dimensional gamma-matrices after the Weyl projection. Integrating out the fermionic matrices, we obtain the determinant

$$\det \mathcal{M}(A) = \int d\Psi d\bar{\Psi} e^{iS_{\text{f},6\text{d}}}, \quad (3.2)$$

which is real. This model can be studied by Monte Carlo simulation using the partition function (2.10), where $\text{Pf}\mathcal{M}(A)$ should be replaced by $\det \mathcal{M}(A)$.

In performing Monte Carlo simulation of the model (2.10) or its $(5+1)$ -dimensional version, the most time-consuming part comes from calculating the contribution from the fermions. Here we consider a simplified model, which can be obtained by replacing the Pfaffian (2.5) or the determinant (3.2) by $\Delta(\alpha)^{2(d-1)}$, which we obtained as the leading contribution when the separation $|\alpha_a - \alpha_b|$ of the eigenvalues of A_0 is large. Note that this amounts to neglecting the terms proportional to the spatial matrices A_i ($i = 1, \dots, d$) in the fermionic action (2.3) or (3.1). Therefore we expect that the simplified model captures the qualitative behaviors of the original models at early times before the expansion of space proceeds much. Thus we arrive at the model

$$\begin{aligned} Z_{\text{VDM}} &= \int \prod_{a=1}^N d\alpha_a \prod_{i=1}^d dA_i \Delta(\alpha)^{2d} \delta \left(\frac{1}{N} \text{tr} (F_{\mu\nu} F^{\mu\nu}) \right) \\ &\times \delta \left(\frac{1}{N} \text{tr} (A_i)^2 - L^2 \right) \theta \left(\kappa L^2 - \frac{1}{N} \text{tr} (A_0)^2 \right), \end{aligned} \quad (3.3)$$

where A_0 is given by (2.11). This model, which we call the VDM model in what follows, can be simulated as easily as the bosonic model. Moreover, it shares important properties with the original supersymmetric models such as the spontaneous symmetry breaking of $\text{SO}(d)$ and expanding behavior of the three-dimensional space after the critical time.

⁶ Similarity of $(5+1)$ -dimensional version and the $(9+1)$ -dimensional version is seen also in the Euclidean IIB matrix model. It was found that $\text{SO}(D)$ symmetry of the D -dimensional model is broken down to $\text{SO}(3)$ symmetry for $D = 10$ [50] and $D = 6$ [62], and various properties associated with the SSB turned out to be common to both models [50].

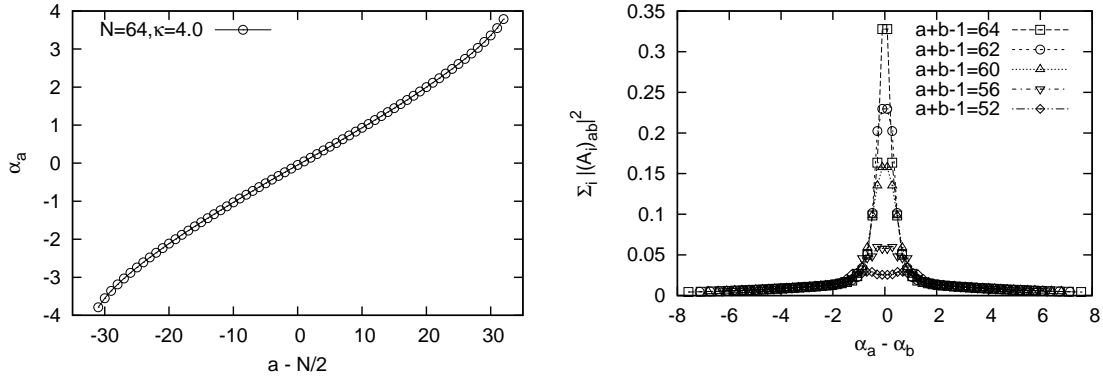


Fig. 1 (Left) The eigenvalues α_a of A_0 with the ordering (2.11) are plotted against its label a for $N = 64$ and $\kappa = 4$. (Right) The magnitude of the off-diagonal elements of A_i defined by the quantity $\sum_i |(A_i)_{ab}|^2$ is plotted against the time separation $\alpha_a - \alpha_b$.

In this paper we study the VDM model in the $d = 5$ case⁷ for simplicity by Monte Carlo simulation. (See appendix B for the details of our simulation.) We set $L = 1$ in (3.3) without loss of generality since it only fixes the scale of the model. In figure 1 (Left) we plot the eigenvalues α_a of A_0 with the ordering (2.11) against its label a for $N = 64$ and $\kappa = 4$. Figure 1 (Right) shows the magnitude of the off-diagonal elements of A_i against the time separation $\alpha_a - \alpha_b$. We find that the off-diagonal element decreases rapidly as one goes away from the diagonal element. Moreover, we observe a nice scaling behavior for sufficiently large $|\alpha_a - \alpha_b|$. The region with small $|\alpha_a - \alpha_b|$ that does not scale includes roughly 8 points. Based on this observation, we choose the block size to be $n = 8$ in this paper.

In figure 2 (Left) we plot $R^2(t)$ against t for $N = 64$ and $\kappa = 4.0$. This plot shows that the space starts to expand at a critical time. In figure 2 (Right) we plot the expectation value $\langle \lambda_i(t) \rangle$ of the five eigenvalues of $T_{ij}(t)$, which shows that the SSB from $SO(5)$ to $SO(3)$ occurs at the critical time.

The definition of the critical time t_c is ambiguous at finite N . As a convenient choice we define it as follows. Note first that the appearance of a gap between $\langle \lambda_3(t) \rangle$ and $\langle \lambda_4(t) \rangle$ signals the SSB of $SO(5)$ to $SO(3)$. Let us therefore define the separation $d_j(t) = \langle \lambda_j(t) \rangle - \langle \lambda_{j+1}(t) \rangle$. Then we find that the symmetric phase can be characterized by $d_1(t) > d_2(t) > d_3(t) > d_4(t)$, while in the broken phase we find $d_2(t) < d_3(t)$. Therefore we define the critical time t_c by the largest value of t' such that $d_1(t) > d_2(t) > d_3(t) > d_4(t)$ holds for $t \leq t'$. For instance, the critical time t_c obtained in this way from figure 2 (Right) is $t_c = -0.8813(2)$ and the extent of space at the critical time is $R^2(t_c) = 0.139(1)$.

In figure 3 (Left) we plot $R^2(t)/R^2(t_c)$ against $(t - t_c)/R(t_c)$ for various values of κ and N , which reveals a nice scaling property⁸ of the function $R^2(t)$. The shift in time is necessary since only the difference $(t - t_c)$ is meaningful. We also normalize all dimensionful quantities

⁷The properties of the $d = 5$ VDM model observed here are confirmed also in the $d = 9$ case. In particular, we observe the SSB from $SO(9)$ to $SO(3)$ at some critical time.

⁸In figure 3 alone, we adjust the critical time t_c slightly from the point defined above for each parameter set (κ, N) in such a way that we optimize the scaling with the data for $\kappa = 4$ and $N = 64$, which are plotted without such adjustment.

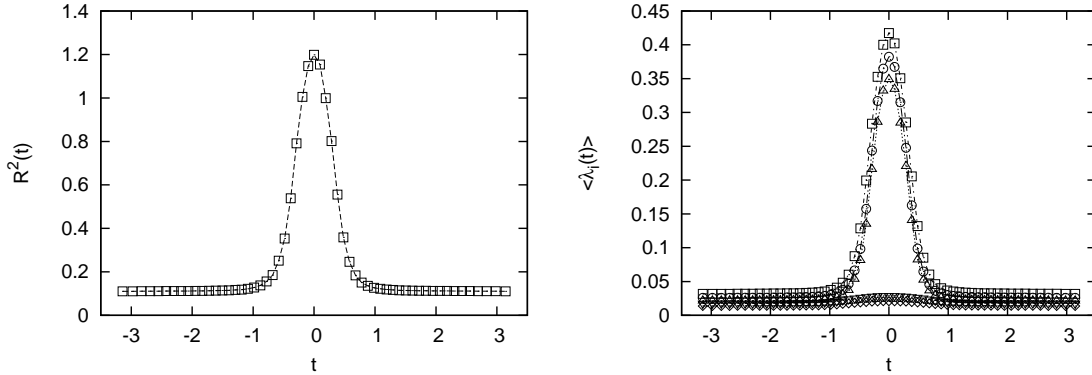


Fig. 2 (Left) The extent of space $R^2(t)$ is plotted against t for $N = 64$ and $\kappa = 4$ with the block size $n = 8$. (Right) The expectation values $\langle \lambda_i(t) \rangle$ of the five eigenvalues of $T_{ij}(t)$ are plotted against t for $N = 64$ and $\kappa = 4$ with the block size $n = 8$. Three of them start to increase rapidly after a critical time. From this behavior we define t_c as explained in the text.

by $R(t_c)$, which represents the size of the universe when it was born. Interestingly, we observe that our data can be fitted well to

$$\frac{R^2(t)}{R^2(t_c)} \equiv f(x) = C + \tilde{C} \exp(-bx) , \quad \text{where } x = \frac{t - t_c}{R(t_c)} . \quad (3.4)$$

(We fix the second coefficient to be $\tilde{C} = 1 - C$ using the constraint $f(0) = 1$, which follows from the definition of $f(x)$.) This is demonstrated in figure 3 (Right), where we plot $R^2(t)/R^2(t_c) - C$ against $(t - t_c)/R(t_c)$ in the logarithmic scale. This exponential growth is reminiscent of the inflation, which is expected to have taken place in the early universe. A similar behavior at early times can be seen also in our preliminary results for the Lorentzian IIB matrix model [63].

Let us discuss how we should take the large- N limit. For that we define the “lattice spacing” ϵ and the “time-extent” Δ by

$$\epsilon \equiv \frac{\delta t}{R(t_c)} , \quad \Delta \equiv \frac{t_p - t_c}{R(t_c)} , \quad (3.5)$$

where δt is the mean separation of the eigenvalues of A_0 and t_p represents the time t at which the extent of space $R(t)$ becomes maximum. (In fact, $t_p = 0$ as one can see from figure 2 due to the time reflection symmetry.) Results for different κ and N correspond to different ϵ and Δ . As κ is increased for a fixed N , the time-extent Δ increases and one can see late-time behaviors more. However, the lattice spacing ϵ increases at the same time, which results in deviations from the scaling behavior due to “lattice artifacts”. Therefore, one needs to increase N as one increases κ to see the scaling behavior at later times. The fact that the scaling behavior extends with increasing N implies that the two cut-offs (2.8) and (2.9) can be removed in the large- N limit. Whether the time-extent Δ diverges in the large- N limit or not is an interesting dynamical question. If it diverges, the $t > 0$ region in figure 2, for instance, becomes invisible in the large- N limit, hence there will be no Big Crunch.

In order to study the late-time behaviors, we need to increase the matrix size further. However, we notice from figure 3 (Left) that the symmetric phase extends more than the

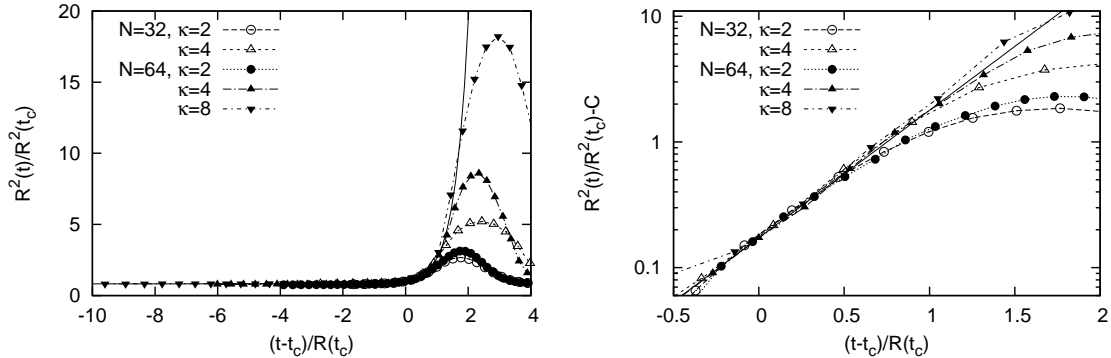


Fig. 3 (Left) The extent of space $R^2(t)/R^2(t_c)$ is plotted against $(t - t_c)/R(t_c)$ for $N = 32$ with $\kappa = 2, 4$ and for $N = 64$ with $\kappa = 2, 4, 8$. The block size for the measurement is taken to be $n = 8$ for all the cases. The solid line represents a fit of the data for $N = 64$ and $\kappa = 4$ to the behavior $R^2(t)/R^2(t_c) = C + (1 - C) \exp(bx)$ with $x = (t - t_c)/R(t_c)$, which yields $C = 0.83(1)$ and $b = 2.3(1)$. (Right) The quantity $R^2(t)/R^2(t_c) - C$ is plotted against $(t - t_c)/R(t_c)$ in the log scale. The constant C is obtained from the exponential fit in the left panel, which corresponds to the solid straight line in this plot.

broken phase with increasing N . Due to this property of the model, it is not efficient to study the late-time behaviors by just increasing the matrix size.

4. Renormalization group method

In this section we propose a new method based on the idea of renormalization group, which enables us to study the late-time behaviors much more efficiently than in a direct approach. Note first that the late-time behaviors are described by the inner part of the matrices A_μ (See figure 4.) if we fix the gauge to (2.11). The corresponding degrees of freedom are given by $\tilde{N} \times \tilde{N}$ Hermitian matrices \tilde{A}_μ , which are defined by

$$(\tilde{A}_\mu)_{ab} = (A_\mu)_{s+a, s+b}, \quad s \equiv \frac{N - \tilde{N}}{2}, \quad (4.1)$$

where the indices a and b run from 1 to \tilde{N} . In principle, we can derive the renormalized theory for \tilde{A}_μ by integrating out the other degrees of freedom in the original matrices A_μ . Once we know the form of the renormalized theory, we can study the late-time behaviors efficiently by simulating the renormalized theory, which has much less degrees of freedom than the original model.

In fact, the properties of the renormalized theory can be investigated by simulating the original model written in terms of A_μ and measuring quantities written in terms of \tilde{A}_μ only. In what follows, we put tildes on all the variables and parameters of the renormalized theory. For instance, corresponding to the cutoffs (2.8), (2.9), we define $\tilde{\kappa}$ and \tilde{L} for the renormalized theory by

$$\tilde{\kappa} \tilde{L}^2 \equiv \left\langle \frac{1}{\tilde{N}} \text{Tr}(\tilde{A}_0)^2 \right\rangle, \quad \tilde{L}^2 \equiv \left\langle \frac{1}{\tilde{N}} \text{Tr}(\tilde{A}_i)^2 \right\rangle, \quad (4.2)$$

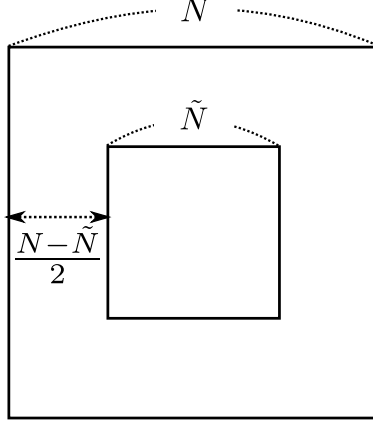


Fig. 4 The basic idea of the renormalization group in the Lorentzian matrix model. If we take the $SU(N)$ basis (2.11), the inner part of the matrices corresponds to the late-time behaviors.

where the symbol $\langle \cdot \rangle$ refers to the VEV with respect to the original model for the whole matrices. Let us also define the quantities

$$\tilde{B} \equiv \left\langle \frac{1}{\tilde{N}} \text{Tr}(\tilde{F}_{ij})^2 \right\rangle, \quad \tilde{E} \equiv \left\langle \frac{2}{\tilde{N}} \text{Tr}(\tilde{F}_{0i})^2 \right\rangle, \quad (4.3)$$

where $\tilde{F}_{\mu\nu} = i[\tilde{A}_\mu, \tilde{A}_\nu]$. Note that $\left\langle \frac{1}{\tilde{N}} \text{Tr}(\tilde{F}_{\mu\nu} \tilde{F}^{\mu\nu}) \right\rangle = \tilde{B} - \tilde{E}$ is not constrained to be zero unlike in the original model (3.3).

In figure 5 the results for $\tilde{\kappa}$, \tilde{L} , \tilde{B} and \tilde{E} obtained from simulations of the original model with $N = 64$ and $\kappa = 4$ are plotted against \tilde{N} . For $\tilde{N} = 64$, which corresponds to the results for the original model, we have $\tilde{\kappa} = 4$, $\tilde{L} = 1$, $\tilde{B} = \tilde{E}$ as it should. Note also that $\tilde{B} \neq \tilde{E}$ for $\tilde{N} < 64$.

Let us then consider an effective theory for the $\hat{N} \times \hat{N}$ Hermitian matrices \hat{A}_μ . (Here and henceforth, we put hats on all the variables and parameters of the effective theory.) We propose

$$Z_{\text{eff}} = \int \prod_{a=1}^{\hat{N}} d\hat{\alpha}_a \prod_{i=1}^d d\hat{A}_i \Delta(\hat{\alpha})^{2d} \delta \left(\frac{2}{\hat{N}} \text{tr}(\hat{F}_{0i})^2 - \hat{E} \right) \delta \left(\frac{1}{\hat{N}} \text{tr}(\hat{F}_{ij})^2 - \hat{B} \right) \\ \times \delta \left(\frac{1}{\hat{N}} \text{tr}(\hat{A}_i)^2 - \hat{L}^2 \right) \theta \left(\hat{\kappa} \hat{L}^2 - \frac{1}{\hat{N}} \text{tr}(\hat{A}_0)^2 \right), \quad (4.4)$$

where \hat{A}_0 is given by (2.11) with all the variables replaced with the ones with hats. Formally, the only difference from the original model (3.3) is that we constrain $\frac{2}{\hat{N}} \text{tr}(\hat{F}_{0i})^2$ and $\frac{1}{\hat{N}} \text{tr}(\hat{F}_{ij})^2$ separately to some values. We study the effective theory for various \hat{N} with the parameters $\hat{\kappa}$, \hat{L} , \hat{E} and \hat{B} chosen to be $\tilde{\kappa}$, \tilde{L} , \tilde{B} and \tilde{E} obtained for $\tilde{N} = \hat{N}$ in figure 5. The results for $\hat{R}^2(\hat{t})$ obtained in this way are plotted in figure 6. We find that they reproduce the late-time behaviors of the original model very well except the region near $\hat{t} = 0$, which is subject to finite “volume” effects anyway. This demonstrates that the effective theory (4.4) indeed captures the late-time behaviors of the original model with much smaller matrix size. Note, in particular, that the symmetric phase, which is not interesting to us, is reduced

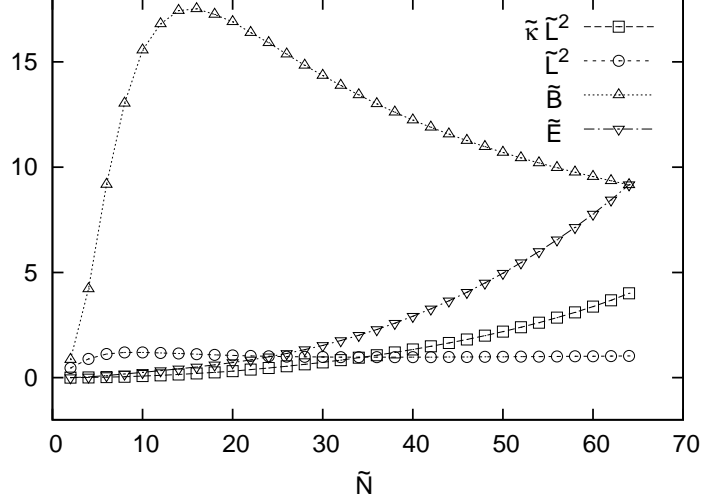


Fig. 5 The results for $\tilde{\kappa} \tilde{L}^2$, \tilde{L}^2 , \tilde{B} and \tilde{E} obtained in the original model with $N = 64$ and $\kappa = 4$ are plotted against \tilde{N} .

considerably compared with the original model. In fact, the results for $\hat{N} = 16$ do not have a symmetric phase at all. We find it remarkable that the data points agree with those for the original model even in this case.

In application of this method, we actually do not know in advance how to choose the parameters $\hat{\kappa}$, \hat{L} , \hat{E} and \hat{B} . This does not spoil the usefulness of the approach at all. In order to show it, we need to answer the question: Can the effective theory (4.4) for arbitrary values of \hat{N} , $\hat{\kappa}$, \hat{L} , \hat{B} and \hat{E} be regarded as a renormalized theory for \hat{A}_μ in the above sense? By counting the number of parameters in the theory, one finds that the answer is generically “yes”. Let us consider the original VDM model with N and κ . Then we define (4.2) and (4.3) for submatrices of size \tilde{N} , which we denote as $\tilde{\kappa}(\tilde{N}; N, \kappa)$, $\tilde{L}(\tilde{N}; N, \kappa)$, $\tilde{B}(\tilde{N}; N, \kappa)$, $\tilde{E}(\tilde{N}; N, \kappa)$. This specifies a renormalized theory. We try to match it with the effective theory (4.4) by setting $\tilde{N} = \hat{N}$. In order to match $\hat{\kappa}$ and \hat{L} with $\tilde{\kappa}(\tilde{N}; N, \kappa)$ and $\tilde{L}(\tilde{N}; N, \kappa)$, we can always make a rescaling of \hat{A}_0 and \hat{A}_i as

$$\tilde{A}_0 = \frac{\sqrt{\tilde{\kappa} \tilde{L}(\tilde{N}; N, \kappa)}}{\sqrt{\hat{\kappa} \hat{L}}} \hat{A}_0, \quad \tilde{A}_i = \frac{\tilde{L}(\tilde{N}; N, \kappa)}{\hat{L}} \hat{A}_i. \quad (4.5)$$

\hat{B} and \hat{E} should be rescaled accordingly, and we require that they should match (after the rescaling) with $\tilde{B}(\tilde{N}; N, \kappa)$ and $\tilde{E}(\tilde{N}; N, \kappa)$ as

$$\begin{aligned} \tilde{B}(\tilde{N}; N, \kappa) &= \left(\frac{\tilde{L}(\tilde{N}; N, \kappa)}{\hat{L}} \right)^4 \hat{B}, \\ \tilde{E}(\tilde{N}; N, \kappa) &= \left(\frac{\sqrt{\tilde{\kappa} \tilde{L}(\tilde{N}; N, \kappa)} \tilde{L}(\tilde{N}; N, \kappa)}{\sqrt{\hat{\kappa} \hat{L}} \hat{L}} \right)^2 \hat{E}. \end{aligned} \quad (4.6)$$

Since we have two arbitrary parameters N and κ at our disposal, we can always choose them to satisfy the two conditions in (4.6). (Strictly speaking, since N can take only integer values, the above statement holds as good approximation for sufficiently large N .)

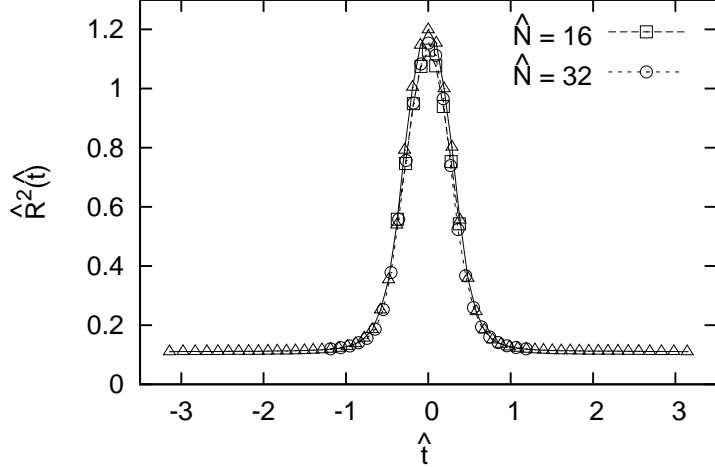


Fig. 6 The extent of space $R^2(t)$ obtained for the effective theory with $N = 16, 32$ is plotted. They agree nicely with the data points (triangles) for the original model with $N = 64$ and $\kappa = 4$, which are also plotted.

Thus we have shown that the effective theory (4.4) for arbitrary values of \hat{N} , $\hat{\kappa}$, \hat{L} , \hat{B} and \hat{E} can be regarded as a renormalized theory of the original model for the submatrices corresponding to late times. For this to work, it was necessary to make the rescaling (4.5). This implies that when one makes a plot like the one in figure 3 (Left) for the effective theory (4.4), one should note that the quantity for the x -axis is related to the corresponding quantity in the renormalized theory through

$$\frac{\tilde{t} - \tilde{t}_{\text{cr}}}{\tilde{R}(\tilde{t}_{\text{cr}})} = \frac{\hat{t} - \hat{t}_{\text{cr}}}{z\hat{R}(\hat{t}_{\text{cr}})}, \quad (4.7)$$

where the time-rescaling parameter z is given by

$$z = \frac{\sqrt{\hat{\kappa}}}{\sqrt{\tilde{\kappa}(\tilde{N}; N, \kappa)}}. \quad (4.8)$$

Therefore we need to plot our results against the right-hand side of (4.7). Since we do not know $\tilde{\kappa}(\tilde{N}; N, \kappa)$ in (4.8) a priori, we determine the parameter z in such a way that the results for the model (4.4) scale with the results for the original model at earlier times. In the next section we will show that this is indeed possible, and the method enables us to study the late-time behaviors of the original model in a much more efficient way.

5. Scaling behaviors in the effective theory

In this section we show how the renormalization group method works by simulating the model (4.4). From now on, we omit the hats on all the variables and the parameters of the model (4.4). We study various values of B and E with $N = 32$, $\kappa = 4$ and $L = 1$ fixed. From a simulation of the original model with $\kappa = 4$ and $N = 32$, we get $B = 7.5$ and $E = 7.6$. The incomplete cancellation $E - B \sim 0.1$ is due to numerical artifacts from finiteness of γ_C in (B1).

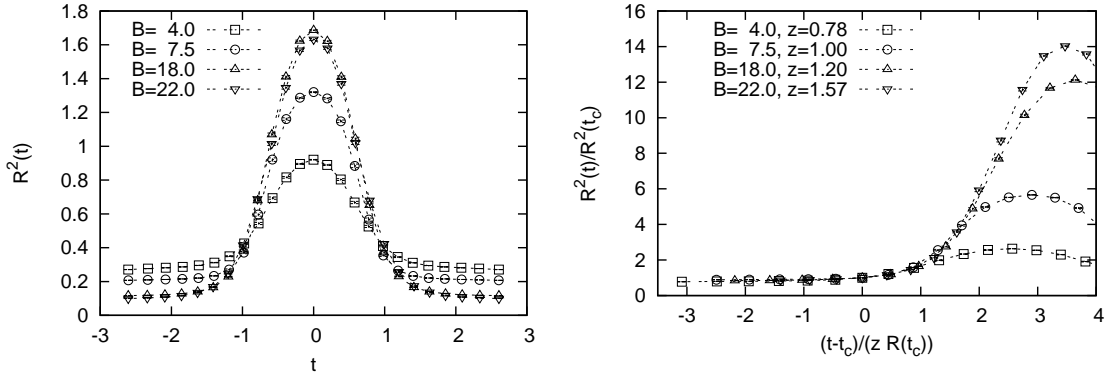


Fig. 7 (Left) The extent of space $R^2(t)$ is plotted against t for various B (including $B = 7.5$, which corresponds to the original model) with fixed $N = 32$, $\kappa = 4$ and $E = 7.6$. (Right) The same data are plotted in physical units. The time-rescaling parameter z is chosen in such a way that the data scale with the results for $B = 7.5$ (corresponding to the original model), for which we use $z = 1$.

In figure 7 (Left) we show our results for the model (4.4) with various B (including $B = 7.5$, which corresponds to the original model) for fixed $E = 7.6$. In figure 7 (Right) we plot the same quantity in physical units. We have introduced the time-rescaling parameter z , which is set to $z = 1$ for $B = 7.5$, which corresponds to the original model, and otherwise it is chosen in such a way that the results scale with the results for $B = 7.5$ at earlier times. Indeed we observe good scaling behavior as anticipated from our arguments in the previous section. We also find that the number of data points in the symmetric phase ($t < t_c$) decreases as B increases. This means that we can use the matrix degrees of freedom more efficiently for the more interesting broken phase. On the other hand, we find that the lattice spacing ϵ increases slowly as we increase B . We have to make sure that the lattice artifacts are kept under control when we increase B .

Figure 8 (Left) shows our results for the model (4.4) with various E (including $E = 7.6$, which corresponds to the original model) for fixed $B = 7.5$. In figure 8 (Right) we plot the same quantity in physical units. The time-rescaling parameter z is set to $z = 1$ for $E = 7.6$, which corresponds to the original model, and otherwise it is chosen in such a way that the results scale with the results for $E = 7.6$ at earlier times. We observe good scaling behavior as anticipated from our arguments in the previous section. We also find that the number of data points in the symmetric phase ($t < t_c$) decreases as E increases. On the other hand, we find that the lattice spacing ϵ and hence the time-extent Δ decrease rapidly as we increase E .

The above results suggest a simple strategy for optimizing B and E . First we increase B from the value for the original model until the lattice spacing ϵ becomes a bit too large. Then we can increase E a little in order to make the lattice spacing ϵ sufficiently small. If necessary, we repeat this procedure a few times until the number of data points in the symmetric phase becomes sufficiently small. This way we can increase the time-extent Δ keeping the lattice spacing sufficiently small with the same matrix size. In figure 9 the region between the two

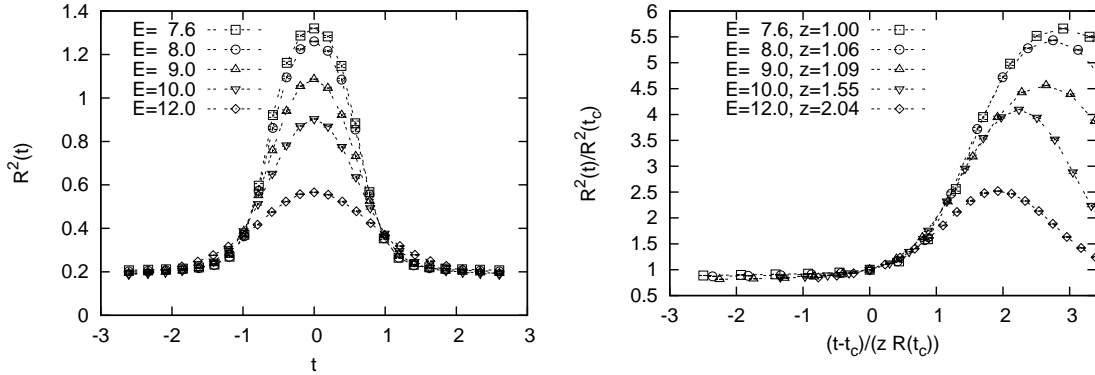


Fig. 8 (Left) The extent of space $R^2(t)$ is plotted against t for various E (including $E = 7.6$, which corresponds to the original model) with fixed $N = 32$, $\kappa = 4$ and $B = 7.5$. (Right) The same data are plotted in physical units. The time-rescaling parameter z is chosen in such a way that the data scale with the results for $E = 7.6$ (corresponding to the original model), for which we use $z = 1$.

curves in the B - E plane correspond to the case with only one data point in the symmetric phase. Within this region, the lattice spacing ϵ decreases as one increases E .

Figure 10 (Left) shows the results for the parameter points (B, E) on the upper curve in figure 9. In order to determine the time-rescaling parameter z , we use the results for the original model with $N = 64$ and $\kappa = 4$ as a reference. The lattice spacing ϵ is larger for larger B and smaller E . We find that it becomes too large for $B = 35$ and $E = 7$ judging from the deviation from the scaling behavior. The scaling region extends until one reaches $B = 29$ and $E = 8$. This gives the maximum time-extent Δ that one can probe using the renormalization group method with $N = 32$.

In figure 10 (Right) we plot $R^2(t)/R^2(t_c) - C$ against $(t - t_c)/(zR(t_c))$, where C is determined by fitting the data in the left panel to an exponential behavior $R^2(t)/R^2(t_c) = C + (1 - C) \exp(bx)$ with $x = (t - t_c)/(zR(t_c))$. We observe a clear straight line behavior providing strong evidence for the exponential expansion of the early universe in the VDM model.

6. Summary and discussions

In this paper we have developed a new method for studying the Lorentzian IIB matrix model for a long time period based on the idea of the renormalization group. The method is tested in a simplified model, which captures the behaviors of the supersymmetric model at early times. We were able to confirm the exponential expansion of the space observed in the simplified model with much smaller matrix size using the new method.

On the conceptual side, we consider it interesting that the idea of the renormalization group works in the Lorentzian matrix model. The renormalization group has been applied to matrix models some time ago by refs. [64–68] and more recently by refs. [69,70]. In particular, ref. [70] studies a Yang-Mills two-matrix model as a simplified model of the Euclidean IIB matrix model. In these papers some elements of the matrices were integrated out explicitly to obtain a renormalized theory for matrices of smaller size. A crucial difference from these

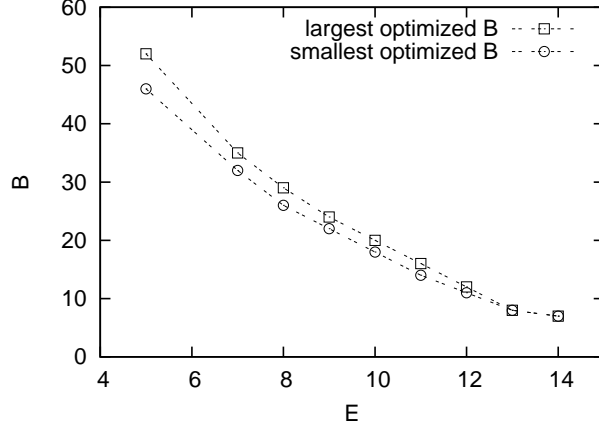


Fig. 9 The largest B (squares) and the smallest B (circles) that correspond to the case with only one data point in the symmetric phase for a fixed E is plotted against E .

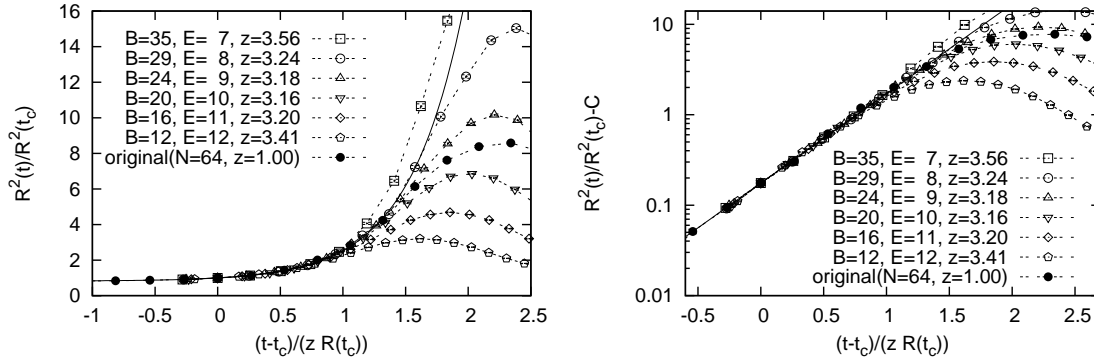


Fig. 10 (Left) The extent of space $R^2(t)$ is plotted in physical units for the parameter points (B, E) on the upper curve in figure 9. The time-rescaling parameter z is fixed by referring to the results for the original model with $N = 64$ and $\kappa = 4$. (Right) $R^2(t)/R^2(t_c) - C$ is plotted in the log scale against $(t - t_c)/(zR(t_c))$, where C is determined by fitting the data in the left panel for $N = 32$, $B = 29$, $E = 8$ to an exponential behavior $R^2(t)/R^2(t_c) = C + (1 - C) \exp(bx)$ with $x = (t - t_c)/(zR(t_c))$, which yields $C = 0.82(1)$ and $b = 2.28(4)$.

works is that we have a notion of time in the Lorentzian matrix model. This allows us to consider a renormalized theory for the submatrices representing the degrees of freedom at later times.

The effective theory for the submatrices representing the later time behaviors contains two extra parameters. We have shown how one can optimize them to probe the late-time behaviors most efficiently. The time-rescaling parameter denoted by z has to be determined by requiring that the results should scale at earlier times with the results obtained for the original model. This procedure becomes more complicated if one applies the present method to the original supersymmetric model since the fermionic action (2.3) or (3.1) contains two terms; one of them being proportional to A_0 and the other being proportional to A_i . The necessity to rescale A_0 and A_i differently as in (4.5) requires us to make the coefficient of

the term proportional to A_i in the fermionic action of the effective theory, a new unknown parameter. This new parameter can be fixed by probing the scaling behavior. Despite this complication, we consider that the renormalization group method is useful in extracting the late-time behaviors in the Lorentzian IIB matrix model. In particular, from the viewpoint of cosmology, we consider it important to confirm the exponential expansion observed in our preliminary results for the Lorentzian IIB matrix model reported in ref. [63], and to see whether it turns into a power-law expansion at later times as suggested there. We hope to report on these issues in future publications.

Acknowledgment

Computation was carried out on PC clusters at KEK and supercomputers SR16000 at YITP, Kyoto University and FX10 at University of Tokyo. The work of Y. I. is supported by Grant-in-Aid for JSPS fellows. The work of S. -W. K. is supported by the National Research Foundation of Korea (NRF) Grant funded by the Korean Government (MEST 2005-0049409 and NRF-2009-352-C00015). The work of J. N. and A. T. is supported by Grant-in-Aid for Scientific Research (No. 20540286, 24540264, and 23244057) from JSPS.

A. Derivation of eq. (2.10)

In this appendix we give a more in-depth derivation of eq. (2.10) than the one given in the original paper [53].

Let us note first that the integrand of the partition function (2.4) involves a phase factor e^{iS_b} . As is commonly done in integrating oscillating functions, we introduce the convergence factor $e^{-\epsilon|S_b|}$ and take the $\epsilon \rightarrow 0$ limit after the integration.

The partition function can then be rewritten as

$$Z = \int dA \int_0^{\Lambda^2} dr \delta\left(\frac{1}{N}\text{Tr}(A_i)^2 - r\right) \theta\left(\kappa r - \frac{1}{N}\text{Tr}(A_0)^2\right) e^{iS_b - \epsilon|S_b|} \text{Pf}\mathcal{M}, \quad (\text{A1})$$

where κ and Λ are the cutoff parameters introduced in (2.8) and (2.9), respectively. Rescaling the variables $A_\mu \rightarrow r^{1/2}A_\mu$ in the integrand, we get

$$Z = \int dA \text{Pf}\mathcal{M}(A) f(S_b) \delta\left(\frac{1}{N}\text{Tr}(A_i)^2 - 1\right) \theta\left(\kappa - \frac{1}{N}\text{Tr}(A_0)^2\right), \quad (\text{A2})$$

where the function $f(S_b)$ is defined by

$$f(S_b) \equiv \int_0^{\Lambda^2} dr r^{9(N^2-1)-1} e^{r^2(iS_b - \epsilon|S_b|)}. \quad (\text{A3})$$

Note that $f(S_b)$ is a complex-valued function with the property $f(-S_b) = f(S_b)^*$. For $|S_b| \ll \frac{1}{\Lambda^4}$, the function can be well approximated by

$$f(S_b) \approx \frac{1}{9(N^2-1)} (\Lambda^2)^{9(N^2-1)}. \quad (\text{A4})$$

For $|S_b| \gtrsim \frac{1}{\Lambda^4}$, the phase of the integrand in (A3) starts to oscillate violently in the region $r \gtrsim 1/\sqrt{|S_b|}$, and hence the integral decreases rapidly in magnitude for increasing $|S_b|$. In

particular, the asymptotic behavior of $f(S_b)$ for $|S_b| \gg \frac{1}{\Lambda^4}$ can be estimated as

$$\frac{f(S_b)}{f(0)} = \Gamma\left(\frac{9}{2}(N^2 - 1) + 1\right) \left(\frac{1}{\Lambda^4 |S_b|}\right)^{\frac{9}{2}(N^2 - 1)} + \mathcal{O}(e^{-\epsilon \Lambda^4 |S_b|}) \quad (\text{A5})$$

by deforming the integration contour in (A3). Recalling eq. (2.6), the condition $|S_b| \ll \frac{1}{\Lambda^4}$ for (A4) can be rewritten as

$$\left| \frac{1}{N} \text{Tr}(F_{\mu\nu} F^{\mu\nu}) \right| \ll \frac{4g^2}{N\Lambda^4}. \quad (\text{A6})$$

Therefore, assuming that the right-hand side $\frac{4g^2}{N\Lambda^4}$ of (A6) becomes small at large N , we may make a replacement

$$f(S_b) \implies \delta\left(\frac{1}{N} \text{Tr}(F_{\mu\nu} F^{\mu\nu})\right) \quad (\text{A7})$$

up to a normalization constant. Rescaling the variables $A_\mu \rightarrow A_\mu/L$, we arrive at eq. (2.10). Within the above approximation, the parameter L simply sets the scale of the model, and we may use $L = 1$ without loss of generality. This is also the case with the VDM model (3.3).

B. Details of Monte Carlo simulation

In this appendix we explain how we actually deal with the simplified model (3.3) in Monte Carlo simulation. Generalization to the effective theory (4.4) is straightforward.

First we replace the delta functions and the step function in (3.3) by Gaussian potentials as

$$\begin{aligned} V_{\text{pot}} = & \frac{1}{2} \gamma_C \left(\frac{1}{N} \text{Tr}(F_{\mu\nu})^2 \right)^2 + \frac{1}{2} \gamma_L \left(\frac{1}{N} \text{Tr}(A_i)^2 - L^2 \right)^2 \\ & + \frac{1}{2} \gamma_\kappa \left(\frac{1}{N} \text{Tr}(A_0)^2 - \kappa L^2 \right)^2 \theta\left(\frac{1}{N} \text{Tr}(A_0)^2 - \kappa L^2\right), \end{aligned} \quad (\text{B1})$$

where the coefficients $\gamma_C, \gamma_L, \gamma_\kappa$ should be taken large enough to fix each observable to the specified value. In actual simulation we have used $\gamma_C \sim 1 \times N^2$ and $\gamma_L = \gamma_\kappa \sim 100 \times N^2$.

Another important issue concerns the spontaneous breaking of the shift symmetry $A_0 \mapsto A_0 + \alpha \mathbf{1}$. For instance, when we try to calculate the expectation value $R^2(t)$ defined in (2.14), the peak of the quantity measured for each configuration fluctuates considerably. This simply reflects the ambiguity in choosing the origin of the time coordinate, and we should fix it somehow before taking the ensemble average. Here we fix it by introducing a potential⁹

$$V_{\text{sym}} = \frac{1}{2} \gamma_{\text{sym}} \left(\frac{1}{N} [\text{Tr}(A_i)^2]_{\text{left}} - \frac{1}{N} [\text{Tr}(A_i)^2]_{\text{right}} \right)^2, \quad (\text{B2})$$

$$[\text{Tr}(A_i)^2]_{\text{left}} = \sum_{i=1}^d \sum_{a+b < N+1} |(A_i)_{ab}|^2, \quad (\text{B3})$$

$$[\text{Tr}(A_i)^2]_{\text{right}} = \sum_{i=1}^d \sum_{a+b > N+1} |(A_i)_{ab}|^2, \quad (\text{B4})$$

⁹ Strictly speaking, the shift symmetry is broken by the traceless condition on A_0 and the cutoff (2.8). However, this breaking is not strong enough to solve the problem.

where the coefficient is typically taken to be $\gamma_{\text{sym}} \sim 100$. We have checked that the results do not alter within error bars for larger values of γ_{sym} .

To summarize, the model we study by Monte Carlo simulation is given by

$$\begin{aligned} Z_{\text{VDM}} &= \int \prod_{a=1}^N d\alpha_a \prod_{i=1}^d dA_i e^{-S_{\text{VDM}}} , \\ S_{\text{VDM}} &= -2d \log \Delta(\alpha) + V_{\text{pot}} + V_{\text{sym}} . \end{aligned} \quad (\text{B5})$$

We apply the Hybrid Monte Carlo (HMC) method to simulate the model (B5). First we rewrite the model by introducing auxiliary variables p_a and $(X_i)_{ab}$ ($a, b = 1, \dots, N$) with the action

$$S_{\text{HMC}} = \frac{1}{2} \sum_a (p_a)^2 + \frac{1}{2} \text{Tr}(X_i)^2 + S_{\text{VDM}}[\alpha, A] . \quad (\text{B6})$$

Here p_a are real variables with the constraint $\sum_a p_a = 0$, whereas X_i are traceless Hermitian matrices. We update all the variables in the model (B6) as follows. First we regard p_a as the conjugate momenta of α_a and X_i as the conjugate momenta of A_i . Then we regard S_{HMC} in (B6) as the Hamiltonian H and solve the classical equations of motion obtained as the Hamilton equations

$$\begin{aligned} \frac{d\alpha_a}{d\tau} &= \frac{\partial H}{\partial p_a} = p_a , & \frac{dp_a}{d\tau} &= -\frac{\partial H}{\partial \alpha_a} = -\frac{\partial S_{\text{VDM}}}{\partial \alpha_a} , \\ \frac{dA_i}{d\tau} &= \frac{\partial H}{\partial X_i} = X_i^* , & \frac{dX_i}{d\tau} &= -\frac{\partial H}{\partial A_i} = -\frac{\partial S_{\text{VDM}}}{\partial A_i} , \end{aligned} \quad (\text{B7})$$

for some fictitious time τ . This part of the algorithm is called the Molecular Dynamics. In solving the Hamilton equations (B7) numerically, we discretize them using the so-called leap-frog discretization, which maintains reversibility with respect to τ . Starting from the previous configuration at $\tau = 0$, we obtain a new configuration at $\tau = \tau_f$ by solving (B7) with the step size $\Delta\tau$ so that $\tau_f = N_\tau \cdot \Delta\tau$, where N_τ is the number of steps. We accept the new configuration with the probability $\min(1, \exp(-\Delta S_{\text{HMC}}))$, where $\Delta S_{\text{HMC}} \equiv S_{\text{HMC}}(\tau_f) - S_{\text{HMC}}(0)$, based on the idea of the Metropolis algorithm to satisfy the detailed balance. The crucial point here is that S_{HMC} is nothing but the Hamiltonian H , which is preserved in the classical dynamics if the equations (B7) are solved exactly. In fact, ΔS_{HMC} is non-zero due to the discretization, but it is a small quantity of order $(\Delta\tau)^2$. Therefore, one can move around efficiently in the configuration space.

Since the auxiliary variables p_a and $(X_i)_{ab}$ appear only as the Gaussian terms in (B6), we can update them independently by using normalized Gaussian random numbers. This procedure of refreshing the conjugate momenta should be done each time we start a Molecular Dynamics procedure. Thus the HMC algorithm as applied to our system can be described as follows.

- (1) Generate initial configurations of $p_a(0)$ and $X_i(0)$ with the Gaussian distribution $e^{-\frac{1}{2}\text{Tr}(X_i)^2}$ and $e^{-\frac{1}{2}\sum_a (p_a)^2}$, respectively.
- (2) Evolve the fields $p_a(\tau)$, $X_i(\tau)$, $\alpha_a(\tau)$ and $A_i(\tau)$ for fictitious time τ_f according to the discretized Molecular Dynamics.
- (3) Accept the obtained configuration of $\alpha_a(\tau_f)$ and $A_i(\tau_f)$ with the probability $\min(1, e^{-\Delta H})$, where $\Delta H = H(\tau_f) - H(0)$.

The HMC algorithm involves two parameters $\Delta\tau$ and τ_f , which can be optimized. (See, for instance, appendix B of ref. [39] for more details.) For fixed τ_f , we have to choose $\Delta\tau$ so that $\Delta\tau \times$ (acceptance rate) is maximized. Typically this is achieved for acceptance rate of 50~60%. Then τ_f can be optimized to minimize the autocorrelation time in units of one step in the Molecular Dynamics.

References

- [1] H. Liu, G. W. Moore and N. Seiberg, *J. High Energy Phys.*, **10**, 031 (2002).
- [2] A. Lawrence, *J. High Energy Phys.*, **11**, 019 (2002).
- [3] G. T. Horowitz and J. Polchinski, *Phys. Rev. D*, **66**, 103512 (2002).
- [4] M. Berkooz, B. Craps, D. Kutasov and G. Rajesh, *J. High Energy Phys.*, **03**, 031 (2003).
- [5] N. Ishibashi, H. Kawai, Y. Kitazawa, and A. Tsuchiya, *Nucl. Phys. B*, **498**, 467 (1997).
- [6] T. Banks, W. Fischler, S. H. Shenker, and L. Susskind, *Phys. Rev. D*, **55**, 5112 (1997).
- [7] R. Dijkgraaf, E. P. Verlinde and H. L. Verlinde, *Nucl. Phys. B*, **500**, 43 (1997).
- [8] D. Z. Freedman, G. W. Gibbons, and M. Schnabl, *AIP Conf. Proc.*, **743**, 286 (2005).
- [9] B. Craps, S. Sethi, and E. P. Verlinde, *J. High Energy Phys.*, **10**, 005 (2005).
- [10] M. Li, *Phys. Lett. B*, **626**, 202 (2005).
- [11] S. R. Das and J. Michelson, *Phys. Rev. D*, **72**, 086005 (2005).
- [12] B. Chen, *Phys. Lett. B*, **632**, 393 (2006).
- [13] J. H. She, *J. High Energy Phys.*, **01**, 002 (2006).
- [14] E. J. Martinec, D. Robbins and S. Sethi, *J. High Energy Phys.*, **08**, 025 (2006).
- [15] T. Ishino and N. Ohta, *Phys. Lett. B*, **638**, 105 (2006).
- [16] T. Matsuo, D. Tomino, W. Y. Wen and S. Zeze, *J. High Energy Phys.*, **11**, 088 (2008).
- [17] D. Klammer and H. Steinacker, *Phys. Rev. Lett.*, **102**, 221301 (2009).
- [18] P. McFadden and K. Skenderis, *Phys. Rev. D*, **81**, 021301 (2010).
- [19] A. Bzowski, P. McFadden and K. Skenderis, *J. High Energy Phys.*, **1304**, 047 (2013).
- [20] J. Nishimura, [arXiv:1405.5904](https://arxiv.org/abs/1405.5904).
- [21] R. J. Szabo, *Class. Quant. Grav.*, **23**, R199 (2006).
- [22] H. Steinacker, *J. High Energy Phys.*, **0712**, 049 (2007).
- [23] H. Steinacker, *Nucl. Phys. B*, **810**, 1 (2009).
- [24] H. Steinacker, *Class. Quant. Grav.*, **27**, 133001 (2010).
- [25] A. P. Polychronakos, H. Steinacker and J. Zahn, *Nucl. Phys. B*, **875**, 566 (2013).
- [26] H. S. Yang, *Int. J. Mod. Phys. A*, **24**, 4473 (2009).
- [27] H. S. Yang, *J. High Energy Phys.*, **0905**, 012 (2009).
- [28] H. S. Yang, [arXiv:1312.0580](https://arxiv.org/abs/1312.0580).
- [29] H. Aoki, N. Ishibashi, S. Iso, H. Kawai, Y. Kitazawa and T. Tada, *Nucl. Phys. B*, **565**, 176 (2000).
- [30] J. Ambjorn, Y. M. Makeenko, J. Nishimura and R. J. Szabo, *J. High Energy Phys.*, **9911**, 029 (1999).
- [31] J. Ambjorn, Y. M. Makeenko, J. Nishimura and R. J. Szabo, *Phys. Lett. B*, **480**, 399 (2000).
- [32] J. Ambjorn, Y. M. Makeenko, J. Nishimura and R. J. Szabo, *J. High Energy Phys.*, **0005**, 023 (2000).
- [33] M. Hanada, H. Kawai and Y. Kimura, *Prog. Theor. Phys.*, **114**, 1295 (2006).
- [34] W. Krauth, H. Nicolai, and M. Staudacher, *Phys. Lett. B*, **431**, 31 (1998).
- [35] P. Austing and J. F. Wheeler, *J. High Energy Phys.*, **04**, 019 (2001).
- [36] H. Aoki, S. Iso, H. Kawai, Y. Kitazawa, and T. Tada, *Prog. Theor. Phys.*, **99**, 713 (1999).
- [37] T. Hotta, J. Nishimura and A. Tsuchiya, *Nucl. Phys. B*, **545**, 543 (1999).
- [38] J. Ambjorn, K. N. Anagnostopoulos, W. Bietenholz, T. Hotta and J. Nishimura, *J. High Energy Phys.*, **07**, 013 (2000).
- [39] J. Ambjorn, K. N. Anagnostopoulos, W. Bietenholz, T. Hotta and J. Nishimura, *J. High Energy Phys.*, **07**, 011 (2000).
- [40] K. N. Anagnostopoulos and J. Nishimura, *Phys. Rev. D*, **66**, 106008 (2002).
- [41] J. Nishimura and G. Vernizzi, *J. High Energy Phys.*, **04**, 015 (2000).
- [42] J. Nishimura and G. Vernizzi, *Phys. Rev. Lett.*, **85**, 4664 (2000).
- [43] J. Nishimura and F. Sugino, *J. High Energy Phys.*, **0205**, 001 (2002).
- [44] H. Kawai, S. Kawamoto, T. Kuroki, T. Matsuo and S. Shinohara, *Nucl. Phys. B*, **647**, 153 (2002).
- [45] T. Aoyama and H. Kawai, *Prog. Theor. Phys.*, **116**, 405 (2006).
- [46] T. Imai, Y. Kitazawa, Y. Takayama and D. Tomino, *Nucl. Phys. B*, **665**, 520 (2003).
- [47] T. Imai, Y. Kitazawa, Y. Takayama and D. Tomino, *Nucl. Phys. B*, **679**, 143 (2004).
- [48] T. Imai and Y. Takayama, *Nucl. Phys. B*, **686**, 248 (2004).
- [49] K. N. Anagnostopoulos, T. Azuma and J. Nishimura, *J. High Energy Phys.*, **1311**, 009 (2013).
- [50] J. Nishimura, T. Okubo and F. Sugino, *J. High Energy Phys.*, **10**, 135 (2011).

-
- [51] J. Ambjorn, J. Jurkiewicz and R. Loll, Phys. Rev. D, **72**, 064014 (2005).
 - [52] H. Kawai and T. Okada, Int. J. Mod. Phys. A, **26**, 3107 (2011).
 - [53] S. -W. Kim, J. Nishimura and A. Tsuchiya, Phys. Rev. Lett., **108**, 011601 (2012).
 - [54] S. -W. Kim, J. Nishimura and A. Tsuchiya, Phys. Rev. D, **86**, 027901 (2012).
 - [55] S. -W. Kim, J. Nishimura and A. Tsuchiya, J. High Energy Phys., **10**, 147 (2012).
 - [56] J. Nishimura and A. Tsuchiya, Prog. Theor. Exp. Phys., **2013**, 043B03 (2013).
 - [57] A. Chatzistavrakidis, H. Steinacker and G. Zoupanos, J. High Energy Phys., **09**, 115 (2011).
 - [58] H. Aoki, Prog. Theor. Phys., **125**, 521 (2011).
 - [59] J. Nishimura and A. Tsuchiya, J. High Energy Phys., **12**, 002 (2013).
 - [60] H. Aoki, J. Nishimura and A. Tsuchiya, J. High Energy Phys., **05**, 131 (2014).
 - [61] M. Fukuma, H. Kawai, Y. Kitazawa and A. Tsuchiya, Nucl. Phys. B, **510**, 158 (1998).
 - [62] T. Aoyama, J. Nishimura and T. Okubo, Prog. Theor. Phys., **125**, 537 (2011).
 - [63] Y. Ito, S. -W. Kim, J. Nishimura and A. Tsuchiya, PoS LATTICE, **2013**, 341 (2013).
 - [64] E. Brezin and J. Zinn-Justin, Phys. Lett. B, **288**, 54 (1992).
 - [65] S. Higuchi, C. Itoi, S. Nishigaki and N. Sakai, Phys. Lett. B, **318**, 63 (1993).
 - [66] S. Higuchi, C. Itoi, S. Nishigaki and N. Sakai, Nucl. Phys. B, **434**, 283 (1995).
 - [67] S. Nishigaki, Phys. Lett. B, **376**, 73 (1996).
 - [68] S. Higuchi, C. Itoi, S. M. Nishigaki and N. Sakai, Phys. Lett. B, **398**, 123 (1997).
 - [69] S. Kawamoto, T. Kuroki and D. Tomino, J. High Energy Phys., **1208**, 168 (2012).
 - [70] S. Kawamoto and D. Tomino, Nucl. Phys. B, **877**, 825 (2013).